Published in final edited form as:
*Mol Cancer Ther*. 2010 October ; 9(10): 2793–2802. doi:10.1158/1535-7163.MCT-10-0477.

# Renal cancer resistance to antiangiogenic therapy is delayed by restoration of angiostatic signaling

**Rupal S. Bhatt**[1,*], **Xiaoen Wang**[2,*], **Liang Zhang**[1], **Michael P. Collins**[3], **Sabina Signoretti**[3,4], **David C. Alsop**[2], **S. Nahum Goldberg**[2], **Michael B. Atkins**[1], and **James W. Mier**[1]

[1]Division of Hematology-Oncology and Cancer Biology Beth Israel Deaconess Medical Center, Boston MA 02215

[2]Department of Radiology, Beth Israel Deaconess Medical Center, Boston MA 02215

[3]Department of Pathology, Brigham and Women's Hospital, Boston MA 02215

[4]Department of Medical Oncology, Dana-Farber Cancer Institute, Harvard Medical School, Boston MA 02215

## Abstract

Treatment of metastatic renal cell cancer (RCC) with antiangiogenic agents that block vascular endothelial growth factor (VEGF) receptor 2 signaling produces tumor regression in a substantial fraction of patients; however resistance typically develops within 6–12 months. The purpose of this study was to identify molecular pathways involved in resistance.

Treatment of mice bearing either 786-0 or A498 human RCC xenografts with sorafenib or sunitinib produced tumor growth stabilization followed by regrowth despite continued drug administration analogous to the clinical experience. Tumors and plasma were harvested at day 3 of therapy and at the time of resistance to assess pathways that may be involved in resistance. Serial perfusion imaging, and plasma and tumor collections were obtained in mice treated with either placebo or sunitinib alone or in combination with intratumoral injections of the angiostatic chemokine CXCL9.

Sunitinib administration led to an early down-modulation of interferon gamma (IFNγ) levels as well as reduction of IFNγ receptor and downstream angiostatic chemokines CXCL9-11 within the tumor. Intratumoral injection of CXCL9 while producing minimal effects by itself, when combined with sunitinib resulted in delayed resistance *in vivo* accompanied by a prolonged reduction of microvascular density and tumor perfusion as measured by perfusion imaging relative to sunitinib alone.

These results provide evidence that resistance to VEGFR therapy is due at least in part to resumption of angiogenesis in association with reduction of IFNγ related angiostatic chemokines, and that this resistance can be delayed by concomitant administration of CXCL9.

### Keywords

Renal cancer; VEGF; CXCL9; antiangiogenic; resistance



**Request for Reprints**: Rupal Bhatt, Division of Hematology Oncology and Cancer Biology, Beth Israel Deaconess Medical Center, Boston MA 02215. Phone 617-735-2062; Fax 617-735-2060; rbhatt@bidmc.harvard.edu.
*These authors contributed equally to this work.

## Introduction

The pathogenesis of renal cell carcinoma (RCC) frequently involves the inactivation of the von Hippel Lindau (VHL) tumor suppressor gene which encodes an E3 ubiquitin ligase complex that targets hypoxia-inducible factor (HIF) for proteasome-mediated degradation. In the setting of VHL inactivation, a large repertoire of hypoxia inducible genes including VEGF and platelet derived growth factor (PDGF) is overexpressed (1). This increase in proangiogenic factors, even in the absence of hypoxia, likely accounts for the nearly unique sensitivity of RCC to treatment with small molecule tyrosine kinase inhibitors (TKIs) of the VEGF receptor (VEGFR) such as sunitinib and sorafenib. Treatment of patients with RCC with these agents frequently leads to tumor regression, but resistance to treatment typically develops within 1 year, substantially limiting their benefit (2–6).

This acquired “evasive” resistance to VEGF pathway inhibition has been observed in multiple preclinical models and tumor types (7). In these settings proposed resistance mechanisms include an increase in alternative proangiogenic factors such as IL-8 and bFGF as seen in the setting of anti-VEGFR2 antibody therapy (8,9). The empty basement membrane sheaths and pericyte changes seen by Mancuso et al could also provide the scaffold for tumor angiogenesis in the resistant setting (10). Other suggested mechanisms include selection of cells that can better tolerate hypoxia (11) and, in the setting of intrinsic resistance to VEGF inhibition, the recruitment of CD11b and Gr1+ bone marrow derived proangiogenic cells (12). Elucidation of the mechanisms underlying the acquired resistance to VEGFR blockade in RCC may contribute to the development of novel therapeutic approaches that could enhance the efficacy of VEGFR inhibitors in this patient population.

Interferon gamma (IFNγ) signaling leads to the production of three angiostatic chemokines, CXCL9-11 (mig, IP-10 and ITAC) (13). These chemokines are highly expressed in RCC relative to normal kidney and have been associated with favorable prognosis in patients with RCC (14,15). Moreover, CXCR3, the receptor for CXCL9-11, is much more highly expressed in RCC than in normal kidney (16) and its expression is associated with improved disease-free survival following nephrectomy (17). Functional studies of CXCL9 and 10 also show that both chemokines exhibit antitumor activity in mouse models of lung cancer and RCC, respectively (18,19). Prior studies from our group have shown that resistance to VEGFR blockade is accompanied by restoration of angiogenesis. We also noted a loss of IFNg regulated chemokines at day 3 of treatment. Consequently, because of the known angiostatic function of these chemokines, we hypothesized that this loss might contribute to the acquired resistance to VEGFR blockade. We investigated this possibility by testing the potential value of restoration and maintenance of angiostatic chemokines in delaying the acquired resistance to VEGFR blockade in murine human tumor xenograft models.

## Materials and Methods

### Reagents

CXCL9 antibody was obtained from R&D (Minneapolis, MN). IFNγR1, CXCL10, CXCL11 and GAPDH antibody for Western Blot were obtained from Abcam (Cambridge, MA). The anti-vinculin antibody was from Sigma (St. Louis, MO). Horse radish peroxidase-conjugated secondary antibodies (goat-anti-mouse, goat-anti-rabbit) were obtained from Cell Signaling Technology (Danvers, MA). For immunohistochemistry (IHC), CD34 was from Abcam, rabbit anti-goat, from Dako, and IFNγR from Santa Cruz.

### Plasma Protein Analysis

The Multiplex bead kit for cytokine measurement was purchased from BioRad Laboratories, Inc (Veenendaal, Netherlands). Standard curves for each mediator were generated, ranging from 2 – 32,000 pg/mL. Plasma samples were incubated with 50 μL of antibody-coupled microsphere sets for 1 hour at room temperature. Freshly diluted secondary detection antibody (25 μL; 1 μg/mL) were added and incubated at room temperature for 1 hour. Streptavidin-phycoerythrin (50 μL; ×1) was added, followed by an incubation for 10 minutes at room temperature. After each step incubation of samples with microsphere sets, secondary detection antibody and streptavidin-phycoerythrin, a filtering step and 3 washing steps using a vacuum manifold were performed. Each well was analyzed on a Bioplex Protein Array System (BioRad Laboratories, Inc) according to the manufacturer's instructions. All protein concentrations are given in picograms (pg) per milliliter.

### Protein Extraction and Western Blot Analysis

Tumor tissues were homogenized in lysis solution (Cell Signaling Technology, Danvers, MA) supplemented with sodium fluoride (10 μM; Fisher) and phenylmethylsulfonyl fluoride (100 μg/ml; Sigma-Aldrich). After sonication for 10 seconds, cell debris was removed by centrifugation at 12,000 *g* for 20 minutes at 4°C. Protein concentration was determined by BCA protein assay reagent (Pierce, Rockford, IL). Lysates were fractionated in either 8 or 12% SDS-polyacrylamide gels, and the separated proteins were transferred to nitrocellulose. The blots were probed for the proteins of interest with specific antibodies followed by a second antibody-horseradish peroxidase conjugate and then incubated with SuperSignal chemiluminescence substrate (Pierce).

### Cell Culture

A498 and 786-O, two VHL deficient human RCC cell lines (20), were obtained from the American Type Culture Collection (ATCC, Manassas, VA) and cultured for less than one month and aliquots were frozen. Fresh frozen aliquots were used for each experiment. A498 was grown in Eagle's Minimum Essential Medium (EMEM). 786-O cells were cultured in RPMI 1640 medium (Cellgro). All media was supplemented with 2mM L-glutamine, 10% fetal calf serum and 1% streptomycin (50μg/ml) and cells were cultured at 37°C with 5% $CO_2$. Growth and morphology of both lines was observed and noted to be consistent with prior descriptions of the lines; no further genetic characterization was performed.

### Tumor xenograft induction

For subcutaneous xenograft tumor models, female athymic nude/beige mice (Charles River Laboratories, MA) were used. The mice were housed and maintained in laminar flow cabinets under specific pathogen-free conditions. All experiments were approved by the Institutional Animal Care and Use Committee at Beth Israel Deaconess Medical Center.

RCC cell lines were harvested from subconfluent cultures by a brief exposure to 0.25% trypsin and 0.02% EDTA. Trypsinization was stopped with medium containing 10% FBS, and the cells were washed once in serum-free medium and resuspended in phosphate buffered saline (PBS). Only suspensions consisting of single cells with greater than 90% viability were used for the injections.

To establish RCC tumor xenografts, 786-O or A498 tumor cells were injected subcutaneously ($1 \times 10^7$ cells) into the flanks of 6–8 week old mice that were of 20 gm average body weight. Tumors developed in > 80% of the mice and were usually visible within a few days of implantation. Sorafenib (80 mg/kg, Bayer) or sunitinib (additive-free, 53.6 mg/kg, Pfizer) was administered 6 out of 7 days per week by gavage beginning when the tumors had grown to a

diameter of 12 mm as per (21,22). Tumors were measured daily while on treatment and the day of resistance recorded. Resistance was defined as an increase tumor diameter by 2mm from its pretreatment size of 12mm. This difference represents the smallest increase in size that could be reproducibly measured by calipers and is roughly analogous to the clinical criteria for resistance (20% growth by RECIST) used in patients. Furthermore, this difference was previously shown to be associated with restored angiogenesis in this model (22). Tumor long and short axes were measured and long axis and tumor volume were followed to determine growth curves. Treatment was continued until tumors grew to 20 mm at which point the mice were sacrificed. Tumor tissue was obtained pre-treatment, during response and at time of resistance for various analyses described below.

### CXCL9 administration

CXCL9 (1 ug in 200ul: R&D systems) was injected into the central portion of tumor xenografts thrice weekly as described previously (18). Control mice received injections of PBS, the vehicle in which the CXCL9 was dissolved. Injections began when tumors reached 12 mm and were given either alone or concomitant with sunitinib as described above. Tumors were measured daily and time to resistance (growth by 2 mm) and 20 mm were ascertained. Tumor tissue was obtained during response and at time of resistance for the various tumor tissue analyses described below.

### Immunohistochemistry

For CD34 analysis, 4um thick sections were prepared from formalin-fixed, paraffin-embedded tumor specimens. Sections were deparaffinized, rehydrated and heated with a pressure cooker to 125°C for 30 seconds in citrate buffer for antigen retrieval. After cooling to room temperature, sections were incubated in 3% hydrogen peroxide for 5 minutes to quench endogenous peroxidase, and then for 20 minutes in Dako serum-free protein block (Dako, Carpinteria, CA). The anti-CD34 antibody (Abcam, Cambridge, MA) was applied at a 1:100 dilution to sections for 1 hour, followed by rabbit anti-goat secondary antibody for 30 minutes. Detection was performed by incubating with Dako EnVision+ System HRP labeled polymer anti-rabbit for 30 minutes, followed by DAB chromogen. Slides were scanned using the Scanscope XT (Aperio Technologies Inc., Visa, CA.) and analyzed using a modified Microvessel analysis algorithm (Aperio Technologies Inc).

For IFNγR staining, frozen OCT sections were used. Sections were fixed in −20C acetone for 5 minutes and then air-dried. Sections were incubated in 3% hydrogen peroxide for 5 minutes to quench endogenous peroxidase. The anti-IFNγR antibody (Santa Cruz Biotechnology, Santa Cruz, CA) was applied at a 1:50 dilution to sections for 1 hour. Detection was performed by incubating with Dako EnVision + System HRP labeled polymer anti-mouse for 30 minutes, followed by DAB chromogen.

### Tumor perfusion imaging

Tumor perfusion imaging (Arterial Spin Labeled (ASL) MRI) was performed as previously described (22). ASL sequence raw data were saved and transferred to the analysis workstation for image reconstruction by using custom software written within the Interactive Data Language (IDL; research Systems, Boulder, Co). The ASL difference image, between average label and control images, was then converted to quantitative tumor perfusion as previously described (23).

To determine tumor perfusion, a region of interest was drawn freehand around the peripheral margin of the tumor by using an electronic cursor on the reference image that was then copied to the perfusion image. The mean blood flow for the tumor tissue within the region of interest was derived, and image window and level were fixed. A 16-color table was applied in 10 mL/

100 g/min increments ranging from 0 to 160 mL/100 g/min, with flow values represented as varying shades of black, blue, green, yellow, red, and purple, in order of increasing perfusion.

## Results

### Modulation of IFNγ signaling with VEGFR inhibitor therapy

786-O derived tumors were implanted into mice as described in the Methods section. Treatment with sunitinib or sorafenib was initiated at a tumor size of 12mm in long axis. Tumors exhibited a period of growth stabilization followed by growth resumption despite continued therapy as previously described (22). Plasma was collected from untreated mice (n=12), day 3 (n=16) and at resistance (n=13). Twenty-seven cytokines were screened using human specific panels and 23 cytokines were screened using murine specific panels. Changes in several cytokines were noted in both the tumor and the stroma at the time of resistance (Supplemental table 1) including a significant decrease in the production of IFNγ (P=0.018 for day 3 vs resistant and 0.0120 for untreated vs. resistant) (Figure 1A). Human cytokines are tumor derived in this system; these findings suggest that tumor-derived IFNγ may be down-modulated with resistance. Other significant changes were observed in several immune cytokines including decreased human GM-CSF and G-CSF and, as previously reported, increased human IL-8 at resistance (24). Significant changes in murine IL-3, IL-4, IL-13, TNFα and GM-CSF were also noted (Figure S1).

To further interrogate this cytokine pathway, expression of IFNγR was measured in the tumors from mice in the absence of therapy or with treatment with either sunitinib or sorafenib. There is abundant expression of IFNγR in untreated tumors and a loss of expression of IFNγR both at day 3 of therapy and at the time of resistance in mice receiving either sorafenib or sunitinib (Figure 1B). These data suggest that a loss of IFNγ signaling can accompany resistance to therapy. Furthermore, immunohistochemical (IHC) analysis demonstrated dramatic downregulation of IFNγR expression in tumors derived from mice that were treated with 3 days of sunitinib as compared to untreated tumors (Figure 1C).

To further define the changes in the IFNγ pathway that accompany resistance to sorafenib and sunitinib, the expression of the angiostatic chemokines regulated by IFNγ was analyzed. Western analysis of the tumors at day 3 of therapy and at the time of resistance shows a loss of all three chemokines (CXCL9-11) relative to untreated tumors (Figure 2). This is consistent with the hypothesis that VEGFR TKI treatment leads to decrease in IFNγ signaling.

### Chemokine administration delays the development of resistance to sunitinib

The treatment induced loss of angiostatic chemokines led to the hypothesis that resistance could be delayed with chemokine replacement. To study this, CXCL9 was injected into the 786-O tumors either alone or concomitant with sunitinib gavage. CXCL9 was selected because of the prior data that this chemokine exhibits activity in murine RCC models (18). Figure 3 shows the growth of tumors treated with vehicle gavage, sunitinib + intratumoral PBS, sunitinib + intratumoral CXCL9, or with intratumoral CXCL9 alone. While CXCL9 alone and treatment with sunitinib alone slows tumor growth, this effect is further enhanced by the combination of sunitinib and injections of CXCL9 (Figure 3). Tumors treated with sunitinib + PBS increased by 2mm in 11.2 ± 1.3 days and this was extended to 18.9 ± 3.2 days with the addition of CXCL9 (p=0.001). Treatment with CXCL9 alone exhibited a similar effect as sunitinib alone (Figure 3). Thus the early administration of CXCL9 with sunitinib delays resistance to sunitinib.

### CXCL9 treatment prolongs antiangiogenic effect of sunitinib

To assess the mechanism by which CXCL9 prolongs the effect of sunitinib; 786-O derived tumors were analyzed at the time of sacrifice. Tumors were harvested from both the sunitinib

+ PBS and sunitinib + CXCL9 groups at the average time when the tumors in the mice treated with sunitinib + PBS reached the 20mm in size (day 43 ± 2.4 post treatment). Figure 4 shows representative IHC sections of CD34 assessment of microvessel density (MVD) of mice treated with vehicle (A), CXCL9 (B), sunitinib + PBS (C) and sunitinib + CXCL9 (D). While CXCL9 itself has no significant effect on MVD, the average MVD of tumors treated with sunitinib + CXCL9 was 40% lower than tumors treated with sunitinib + PBS (P =0.014).

To further assess the angiogenic capability of the treated tumors, serial tumor perfusion imaging by ASL MRI was performed. Figure 5A shows a time course of tumor (786-O) perfusion in a mouse treated with vehicle, CXCL9, sunitinib + PBS or sunitinib + CXCL9. While sunitinib + PBS and sunitinib + CXCL9 produced initial loss of perfusion compared with control followed by recovery of perfusion at the time of resistance, treatment with sunitinib + CXCL9 suppressed perfusion for longer and to a greater extent. Resumption of perfusion was seen on week 3 (day 22–26) and was significant by week 6 (day 42–46) (P=0.03) in sunitinib + PBS treated mice, while mice treated with sunitinib + CXCL9 exhibited a greater reduction in tumor perfusion that was maintained at both week 3 (day 22–26) and week 6 (day 42–46) of therapy (P=0.03 and 0,04 respectively). In contrast to tumor perfusion in mice treated with sunitinib + PBS, tumor perfusion at time of resistance to sunitinib + CXCL9 never attained the pretreatment perfusion levels. These observations are consistent with the CD34 IHC data. Tumor perfusion exhibited little change over time in either the PBS alone and CXCL9 alone treated mice (Figure 5 A and B).

### CXCL9 restoration delays resistance in a second xenograft model

To confirm these findings and extend them to another tumor model, mice bearing xenograft tumors derived from A498 cells were treated with sunitinib + PBS or sunitinib + CXCL9. As noted in the 786-O derived tumors, CXCL9 when initiated with sunitinib extended the duration of relative tumor stability as measured by time to increase by 2mm. Tumors treated with the combination of CXCL9 and sunitinib showed a 39.8 ± 6.1 day compared to 22.2 ± 4.1 day period of stability for sunitinib + PBS (P=0.0008) (Figure 6A). CXCL9 itself also slowed tumor growth but not to as great an extent as the sunitinib containing treatments. Serial ASL MRI was performed on mice treated with, vehicle, CXCL9 alone, sunitinib + PBS or sunitinib + CXCL9. Both administration of sunitinib + PBS ($P \leq 0.001$) and CXCL9 alone (P=0.001) significantly reduced perfusion relative to vehicle (Supplemental Figure). Representative images show that the combination of sunitinib + CXCL9 resulted in a greater reduction in tumor blood flow and lower tumor perfusion at all time points relative to sunitinib + PBS (Figure 6B and Supplemental Figure, P=0.001). As in 786-O tumors, ASL MRI measured tumor perfusion in sunitinib + CXCL9 treated mice never returns to the pretreatment perfusion level. Levels of IFNγR and CXCL9 are down-modulated in the A498 tumors with exposure to sunitinib (Figure 6C). However in contrast to 786-O tumors, the majority of A498 tumors, exhibit increases in these molecules at the time of resistance to sunitinib. This early, but not sustained loss of angiostatic chemokines is consistent with the need for early supplementation of sunitinib with CXCL9.

## Discussion

Treatment of patients with the VEGFR TKIs sorafenib and sunitinib can lead to periods of tumor stability but resistance to therapy is inevitable. We have used a mouse model to define mechanisms by which resistance develops and have found that components of the IFNγ signaling pathway are lost with sunitinib or sorafenib therapy. Our data also show that CXCL9 treatment delays resistance to sunitinib in 786-O and A498 derived tumors and that one mechanism by which this occurs is by prolongation of antiangiogenic effects of sunitinib. These

data suggest that angiostatic pathways are suppressed as a result of VEGFR TKI therapy and set the stage for the subsequent development of resistance to therapy.

In the setting of VEGFR inhibition, RCC tumors undergo extensive necrosis (22). In the setting of this necrosis and accompanying hypoxia/nutrient deprivation, tumors may undergo compensatory changes including the induction of salvage angiogenesis pathways. We propose that the environmental stress resultant from a rapid and dramatic reduction in tumor vasculature and VEGFR signaling is particularly conducive to the development of such molecular changes. We hypothesize that one of these molecular changes is the loss of IFNγR and that this loss is linked to the downmodulation of angiostatic chemokines. Thus, this revascularization of VEGF-deprived tumors is likely *physiologically distinct from de novo* angiogenesis.

Within just a few days of therapy, RCC xenografts appear particularly vulnerable to agents that could prevent salvage angiogenesis. In fact, we show an early loss (by day 3 of treatment) of IFNγR and CXCL9, which led to our hypothesis that treatment with CXCL9, must be administered early. Thus we administered sunitinib and CXCL9 concurrently in an effort to overcome possible changes resulting from this early loss of angiostasis. While other recently published studies have shown that antiangiogenic therapy can lead to increased production of angiogenic molecules and increased invasiveness and metastatic potential (25,26), we show that antiangiogenic therapy also leads to down modulation of angiostatic signaling.

CXCR3, the receptor for CXCL9, is expressed on both tumor cells and endothelium. CXCR3 signaling in other tumor types has pro-invasive properties (27). By contrast, RCC xenografts in our models did not show accelerated growth compared to untreated tumors when injected with single agent CXCL9. This is consistent with the finding that CXCR3 expression confers a favorable prognosis in patients with localized RCC (28). Future studies could explore CXCR3 expression in the tumors including the spliced subtype expression as well as the potential role for direct effects of CXCL9 on tumor cells. Additionally, CXCL9 has been shown to function in leukocyte activation via its interaction with CXCR3 on Th1 cells. While our experiments used immunocompromised mice, there remains the possibility that CXCL9 also recruits immune cells to the tumor, although in preliminary experiments we did not see evidence of increased lymphocyte recruitment to the tumors (data not shown). Exclusion of an immune role for CXCL9 would likely require studies in more severely immunodeficient mice such as RAG KO mice. Finke et al have noted an increase in type I IFNγ producing cells after treatment with sunitinib (29). Further studies will be required to understand the relationship between this finding and the loss of IFNγR signaling that we have seen.

To measure tumor vasculature, we have analyzed tumor expression of CD34 by IHC and performed tumor perfusion imaging using ASL MRI. We have shown here that CD34 staining correlates with ASL MRI perfusion, giving us confidence to use this imaging modality to assess response and resistance to antiangiogenic therapy. One noteworthy advantage of ASL MRI over CD34 is that it enables serial imaging of tumors as opposed to comparing distinct tumors removed from different animals at different time points. While plasma biomarker analyses have shown that there are changes in plasma cytokines that may predict for antitumor activity (30), there are advantages to having a visual representation of the angiogenic status of a tumor in an individual patient. This could provide early clues to the timing and means by which escape from therapy occurs. Our data show that a hallmark of sunitinib treatment is dramatically reduced tumor perfusion followed by a restoration of tumor perfusion accompanied by tumor regrowth. Prior work from our group has shown similar findings with sorafenib treatment (22). We did note, however, that the restored tumor perfusion at the time a resistance never reaches the pretreatment levels. This finding suggests that angiogenesis-independent factors may also contribute to resistance to VEGFR blockade. For example, metabolic changes in a

tumor may occur that limit its oxygen requirements relative to the treatment naïve setting (31).

The biological significance of the downmodulation of CXCL9 and the IFNγR noted shortly after beginning treatment with a VEGFR antagonist is unclear. The fact that these angiostatic molecules are expressed by tumor cells in untreated mice and even overexpressed in some tumors that have developed resistance to sunitinib indicates that their presence is not an absolute deterrent to tumor growth and vascularization. This may be especially true in the resistant setting, in which new angiogenic pathways may dominate over the angiostatic forces. CXCL9 initiated concurrently with the sunitinib, however, prolonged the duration of sunitinib-induced growth arrest and delayed the revascularization and resumption of tumor perfusion that otherwise rapidly ensues in mice treated with sunitinib alone. This observation indicates that the early phases of tissue remodeling induced by VEGFR blockade are affected by the presence of CXCL9 and that the disappearance of this chemokine from the tissue facilitates the re-establishment of the tumor microcirculation and the development of resistance to VEGFR antagonists. Thus, the early loss of CXCL9 and IFNγR expression seen in the A498 tumors is likely the dominant predictor of the utility of chemokine supplementation and the observation that these molecules are reexpressed at resistance may indicate that other pro-angiogenic factors can be sufficient to mediate tumor growth even in the presence of enhanced expression of angiostatic factors such as CXCL9.

While intratumoral CXCL9 injection validates the concept that sunitinib resistance can be delayed with CXCR3 ligands, this method of delivery is not amenable to clinical practice. Future studies that would enable translation to the clinical setting could involve the application of a CXCR3 agonist. Additionally, the potential use of systemic CXCL9 could be explored as could treatment of patients with IFNγ or IFNγ inducing agents such as IL-12. Although we find that tumor cells lose IFNγR and may not be able to respond to IFNγ treatment by producing CXCL9-11, it is possible that other non-tumor cell types maintain the ability to upregulate the angiostatic chemokines in response to IFNγ despite antiangiogenic therapy. We are currently exploring this issue.

The inability to sustain the initial tumor stabilization or regression induced by VEGF pathway blockers is arguably the most vexing problem now encountered by oncologists who care for patients with RCC. Our studies suggest that relative loss of CXCL9 is one of the molecular mechanisms that curtail the initial effectiveness of VEGFR blockers. Future studies with augmentation of angiostatic pathways might lead to the elucidation of therapeutic approaches that extend the effectiveness of sunitinib, sorafenib or other VEGF pathway blockers in RCC and possibly other tumors.

## Supplementary Material

Refer to Web version on PubMed Central for supplementary material.

## Acknowledgments

**Supported by:** DF/HCC Kidney Cancer SPORE: 2 P50 CA101942 VHL Family Alliance Grant, Clinical Investigator Training Program: Beth Israel Deaconess Medical Center - Harvard/MIT Health Sciences and Technology, in collaboration with Pfizer Inc. and Merck & Co (RSB), and a grant from the National Comprehensive Cancer Network, Jenkintown PA

## References

1. Kaelin WG Jr. The von Hippel-Lindau protein, HIF hydroxylation, and oxygen sensing. Biochem Biophys Res Commun 2005;338:627. [PubMed: 16153592]

2. Motzer RJ, Michaelson MD, Redman BG, et al. Activity of SU11248, a multitargeted inhibitor of vascular endothelial growth factor receptor and platelet-derived growth factor receptor, in patients with metastatic renal cell carcinoma. J Clin Oncol 2006;24:16–24. [PubMed: 16330672]
3. Motzer RJ, Rini BI, Bukowski RM, et al. Sunitinib in Patients With Metastatic Renal Cell Carcinoma. JAMA 2006;295:2516–2524. [PubMed: 16757724]
4. Motzer RJ, Hutson TE, Tomczak P, et al. Sunitinib versus interferon alfa in metastatic renal-cell carcinoma. N Engl J Med 2007;356:115–124. [PubMed: 17215529]
5. Escudier B, Eisen T, Stadler WM, et al. TARGET Study Group. Sorafenib in advanced clear-cell renal-cell carcinoma. N Engl J Med 2007;356:125–134. [PubMed: 17215530]
6. Rini BI, Atkins MB. Resistance to targeted therapy in renal-cell carcinoma. Lancet Oncol 2009;10:992–1000. [PubMed: 19796751]
7. Bergers G, Hanahan D. Modes of resistance to anti-angiogenic therapy. Nat Rev Cancer 2008;8:592–603. [PubMed: 18650835]
8. Casanovas O, Hicklin D, Bergers G, Hanahan D. Drug resistance by evasion of antiangiogenic targeting of VEGF signaling in late-stage pancreatic islet tumors. Cancer Cell 2005;8(4):299–309. [PubMed: 16226705]
9. Mizukami Y, Jo WS, Duerr EM, Gala M, Li J, Zhang X, Zimmer MA, Iliopoulos O, Zukerberg LR, Kohgo Y, Lynch MP, Rueda BR, Chung DC. Induction of interleukin-8 preserves the angiogenic response in HIF-1alpha-deficient colon cancer cells. Nat Med 2005;11:992–997. [PubMed: 16127434]
10. Mancuso MR, Davis R, Norberg SM, et al. Rapid vascular regrowth in tumors after reversal of VEGF inhibition. J Clin Invest 2006;116:2610–2621. [PubMed: 17016557]
11. Yu JL, Rak JW, Coomber BL, Hicklin DJ, Kerbel RS. Effect of p53 status on tumor response to antiangiogenic therapy. Science 2002;295:1526–1528. [PubMed: 11859195]
12. Shojaei F, Wu X, Malik AK, et al. Tumor refractoriness to anti-VEGF treatment is mediated by CD11b +Gr1+ myeloid cells. Nat Biotechnol 2007;25:911–920. [PubMed: 17664940]
13. Strieter RM, Burdick MD, Mestas J, Gomperts B, Keane MP, Belperio JA. Cancer CXC chemokine networks and tumour angiogenesis. Eur J Cancer 2006;42:768–778. [PubMed: 16510280]
14. Kondo T, Nakazawa H, Ito F, et al. Favorable prognosis of renal cell carcinoma with increased expression of chemokines associated with a Th1-type immune response. Cancer Sci 2006;97:780–786. [PubMed: 16863511]
15. Kondo T, Ito F, Nakazawa H, Horita S, Osaka Y, Toma H. High expression of chemokine gene as a favorable prognostic factor in renal cell carcinoma. J Urol 2004;171:2171–2175. [PubMed: 15126779]
16. Suyama T, Furuya M, Nishiyama M, et al. Up-regulation of the interferon gamma (IFN-gamma)-inducible chemokines IFN-inducible T-cell alpha chemoattractant and monokine induced by IFN-gamma and of their receptor CXC receptor 3 in human renal cell carcinoma. Cancer 2005;103:258–267. [PubMed: 15578685]
17. Klatte T, Seligson DB, Leppert JT, et al. The chemokine receptor CXCR3 is an independent prognostic factor in patients with localized clear cell renal cell carcinoma. J Urol 2008;179:61–66. [PubMed: 17997430]
18. Pan J, Burdick MD, Belperio JA, et al. CXCR3/CXCR3 ligand biological axis impairs RENCA tumor growth by a mechanism of immunoangiostasis. J Immunol 2006;176:1456–1464. [PubMed: 16424173]
19. Arenberg DA, Kunkel SL, Polverini PJ, et al. Interferon-gamma-inducible protein 10 (IP-10) is an angiostatic factor that inhibits human non-small cell lung cancer (NSCLC) tumorigenesis and spontaneous metastases. J Exp Med 1996;184:981–992. [PubMed: 9064358]
20. Iliopoulos O, Kibel A, Gray S, Kaelin WG Jr. Tumour suppression by the human von Hippel-Lindau gene product. Nat Med 1995;8:822–826. [PubMed: 7585187]
21. Sabir A, Schor-Bardach R, Wilcox CJ, et al. Perfusion MDCT enables early detection of therapeutic response to antiangiogenic therapy. AJR Am J Roentgenol 2008;191:133–139. [PubMed: 18562736]
22. Schor-Bardach R, Alsop DC, Pedrosa I, et al. Does arterial spin-labeling MR imaging-measured tumor perfusion correlate with renal cell cancer response to antiangiogenic therapy in a mouse model? Radiology 2009;251:731–742. [PubMed: 19474376]

23. Alsop DC, Detre JA. Reduced transit-time sensitivity in noninvasive magnetic resonance imaging of human cerebral blood flow. J Cereb Blood Flow Metab 1996;16:1236–1249. [PubMed: 8898697]
24. Huang D, Ding Y, Zhou M, Rini BI, et al. Interleukin-8 mediates resistance to antiangiogenic agent sunitinib in renal cell carcinoma. Cancer Res 2010;70:1063. [PubMed: 20103651]
25. Pàez-Ribes M, Allen E, Hudock J, et al. Antiangiogenic therapy elicits malignant progression of tumors to increased local invasion and distant metastasis. Cancer Cell 2009;15:220–231. [PubMed: 19249680]
26. Ebos JM, Lee CR, Cruz-Munoz W, Bjarnason GA, Christensen JG, Kerbel RS. Accelerated metastasis after short-term treatment with a potent inhibitor of tumor angiogenesis. Cancer Cell 2009;15:232–239. [PubMed: 19249681]
27. Zipin-Roitman A, Meshel T, Sagi-Assif O, et al. CXCL10 promotes invasion-related properties in human colorectal carcinoma cells. Cancer Res 2007;67:3396–3405. [PubMed: 17409450]
28. Klatte T, Seligson DB, Leppert JT, et al. The chemokine receptor CXCR3 is an independent prognostic factor in patients with localized clear cell renal cell carcinoma. J Urol 2008;179:61–66. [PubMed: 17997430]
29. Finke JH, Rini B, Ireland J, et al. Sunitinib reverses type-1 immune suppression and decreases T-regulatory cells in renal cell carcinoma patients. Clin Cancer Res 2008;20:6674–6682. [PubMed: 18927310]
30. Ebos JM, Lee CR, Bogdanovic E, et al. Vascular endothelial growth factor-mediated decrease in plasma soluble vascular endothelial growth factor receptor-2 levels as a surrogate biomarker for tumor growth. Cancer Res 2008;68:521–529. [PubMed: 18199548]
31. Aragonés J, Schneider M, Van Geyte K, et al. Deficiency or inhibition of oxygen sensor Phd1 induces hypoxia tolerance by reprogramming basal metabolism. Nat Genet 2008;40:170–180. [PubMed: 18176562]

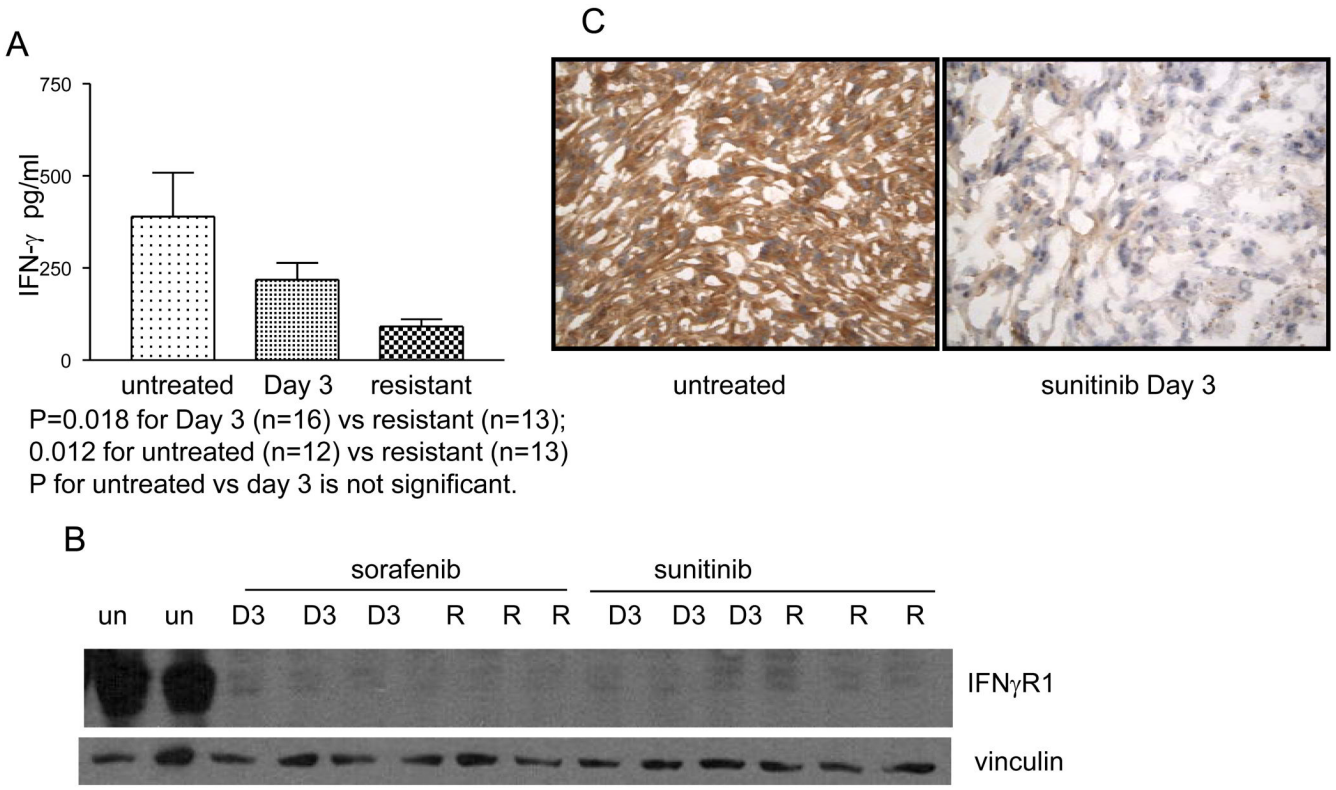


**Figure 1.**

Plasma analysis of mice harboring tumors that were untreated (389.8+/−118.6pg/ml) (n=12 mice) Day 3 after initiation of sorafenib (218.5+/−45.5pg/ml) (n=16 mice) and that were resistant (90.76+/−20.0pg/ml) (n=13 mice) is shown (A). In the setting of resistance to sorafenib, plasma IFNγ decreases (P=0.018 for Day 3 vs resistant and for 0.012 for untreated vs resistant). Figure 1B is a Western analysis showing that IFNγR is down modulated at day 3 of therapy with sorafenib or sunitinib (D3) and at the time of resistance (R) as compared to untreated tumors (un). Results from tumors harvested from 2–3 different mice treated with the described conditions are shown. Figure 1C shows a representative IHC stain for IFNγR in an untreated tumor as compared to a tumor that was treated with sunitinib for 3 days. Staining is present in the untreated tumor and absent in the treated tumor.

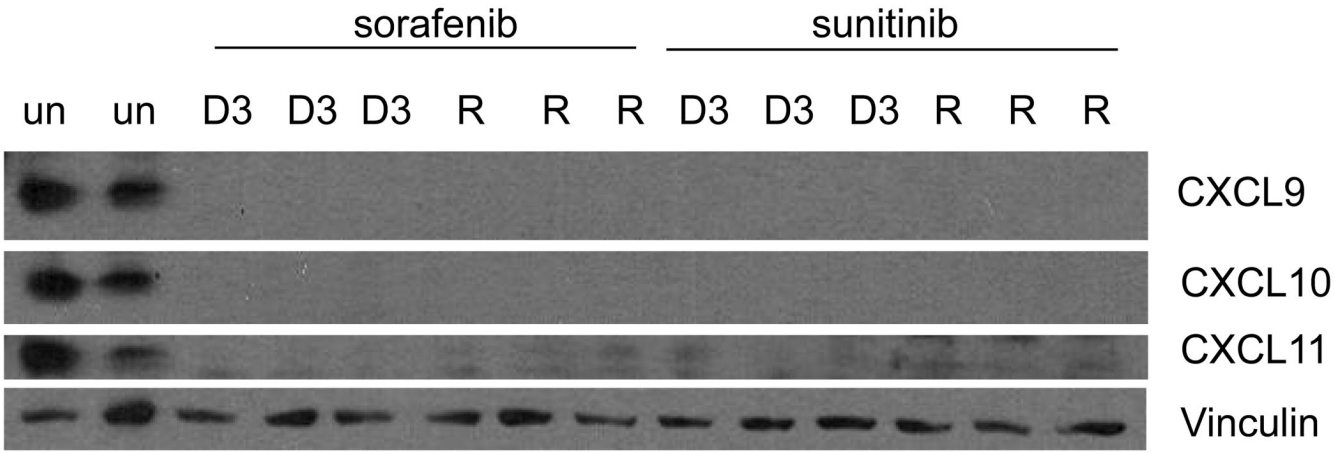


**Figure 2.**
Western analysis showing that CXCL9-11 are down modulated at day 3 of therapy (D3) with sorafenib or sunitinib and at the time of resistance (R) as compared to untreated tumors (un). Results from 2–3 representative tumors harvested from different mice treated with the described conditions are shown.

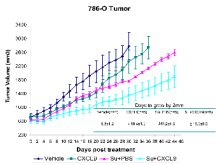


**Figure 3.**

Growth curves depicting average tumor volume of 786-O derived tumors from mice treated with vehicle gavage (n=3), sunitinib + CXCL9 (n=5), sunitinib+ PBS (n=5), or intratumoral CXCL9 (n=5), are shown with standard error. As compared to vehicle treated controls or sunitinib treated mice, the growth of tumors treated with sunitnib+ CXCL9 exhibit a longer time to resistance shown in the accompanying table (#vehicle vs. sunitinib + PBS: p=0.002, *vehicle vs. CXCL9: p=0.016, § sunitinib + PBS vs. sunitinib + CXCL9 p=0.001). Comparisons were performed by Student's T-test.

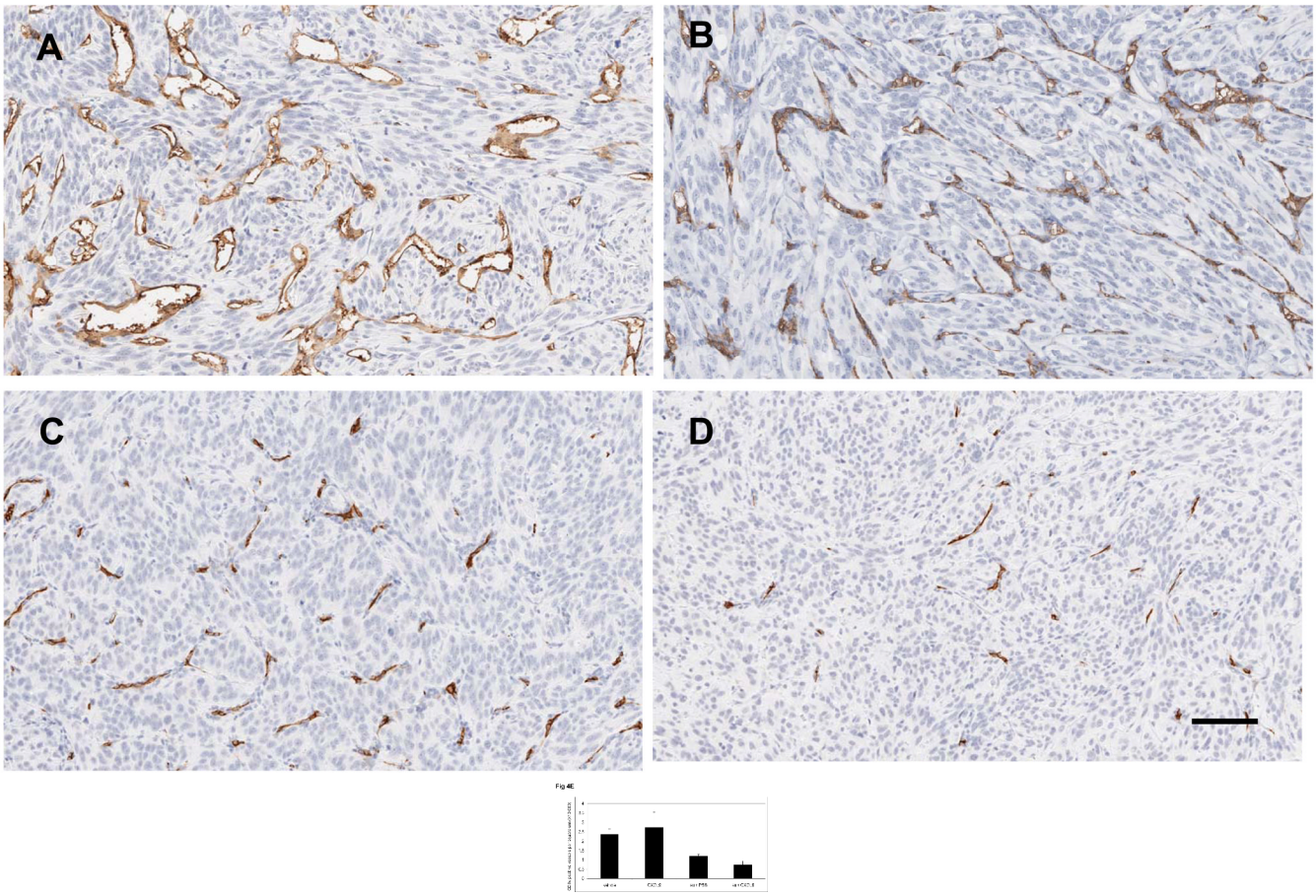




**Figure 4.**

Tumor CD34 IHC at the time of sacrifice is shown in the following conditions: A. vehicle, B. CXCL9, C. sunitinib + PBS, D. sunitinib + CXCL9. Mice treated with sunitinib + PBS (n=3) were sacrificed when they reached 20mm in long axis and mice treated with sunitinib + CXCL9 (n=4) were sacrificed at the average day that the sunitinib treated mice were sacrificed. Mice treated with vehicle (n=3) and CXCL9 alone (n=3) were sacrificed at 20mm. The average MVD was quantified and is shown (E). P=0.014 for the comparison of sunitinib + PBS vs sunitinib + CXCL9. The scale bar is 100uM.

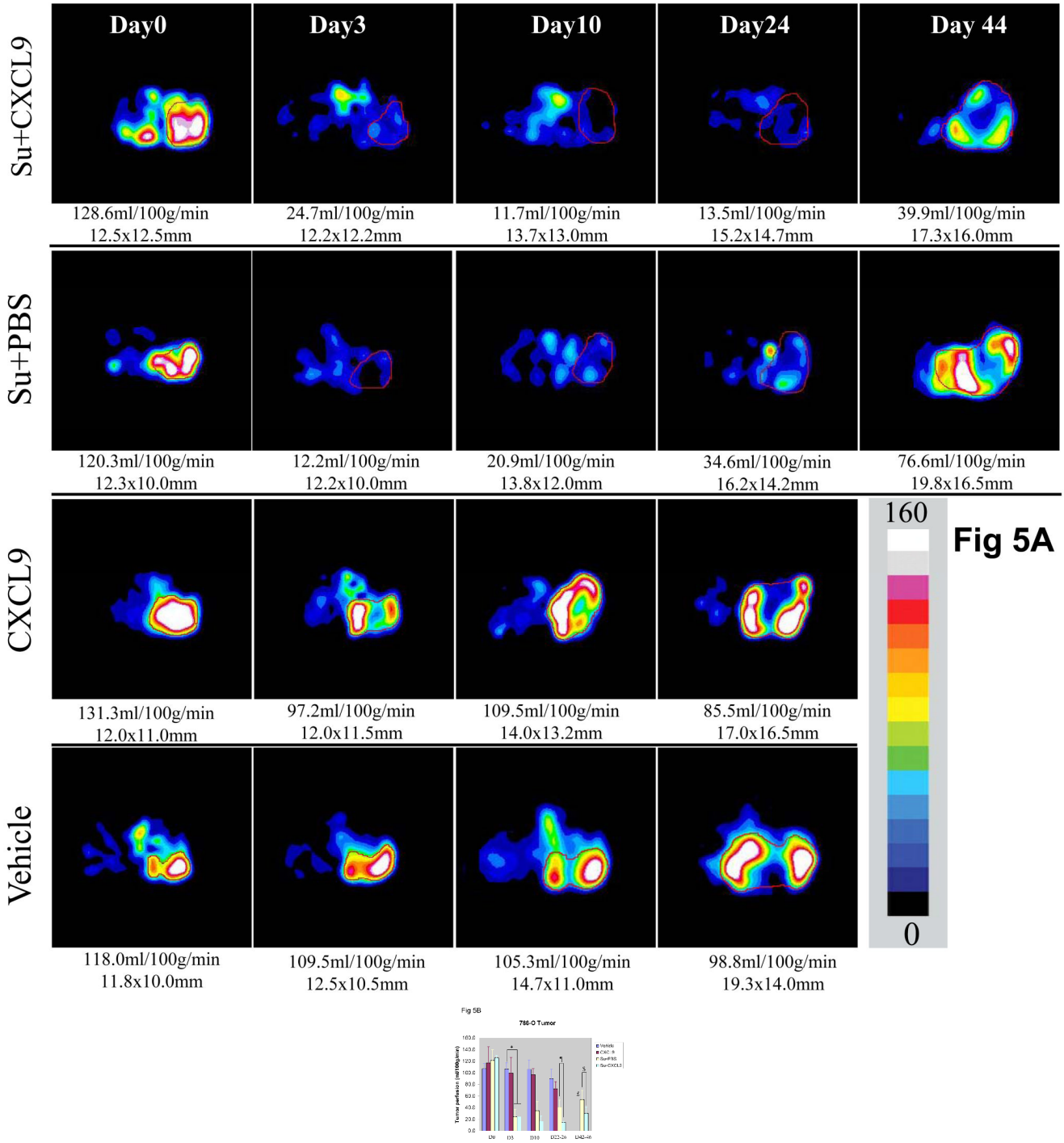


**Figure 5.**

Serial tumor perfusion in a representative tumor treated with Vehicle as control, CXCL9 alone, sunitinib+ PBS, or sunitinib + CXCL9 as measured by ASL MRI is shown in A. The region of tumor is highlighted with red line in each image. The tumor size was measured with long and short axes (in mm) and the mean blood flow (in ml/100g/min) are shown below each image. Color scale represents range of perfusion values from 0 to 160ml/100g/min. In B, average perfusion with standard error is shown (n≥3 mice in all arms). The mice treated with sunitinib

+ PBS exhibited decreased perfusion that began to resume by week 3 (*P=0.04 for comparison of vehicle vs sunitinib treated mice, £ P=0.03 for comparison of day 3 vs day 45 of therapy with sunitinib + PBS). In contrast, mice treated with sunitinib + CXCL9 exhibited a greater reduction in tumor perfusion than with sunitinib + PBS that was maintained at week 3 (Day 22–26) and week 6 (Day 42–46) (¶ P=0.03 and $P=0.04 respectively).

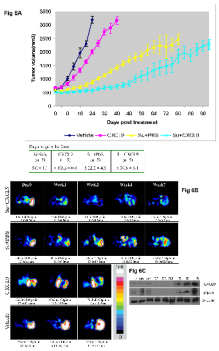

**Figure 6.**

Growth curves of average volume of A498 derived xenograft tumors treated with sunitinib + PBS, sunitinib, + CXCL9, CXCL9, or vehicle are shown with standard error (n=5 in all arms) (A). As compared to untreated controls or sunitinib treated mice, the growth of tumors treated with sunitinib+ CXCL9 exhibit a longer time to grow by 2mm shown in the accompanying Table and a prolonged time of overall tumor growth (days of tumor growth from 12mm to 14mm: sunitinib + PBS vs. sunitinib + CXCL9, §P=0.0008). CXCL9 also slowed tumor growth but to a lesser extent than sunitinib + CXCL9 (*P<0.0001 for CXCL9 vs vehicle, #P<0.0001 for CXCL9 vs sunitinib + CXCL9). Figure 6B shows a representative set of perfusion images from a set of mice treated with Vehicle as control, CXCL9 alone, sunitinib + PBS or sunitinib + CXCL9 (this figure is representative of 3 mice per arm). The region of tumor is highlighted with red line in each image. The tumor size was measured with long and short axes (in mm) and the mean blood flow (in ml/100g/min) are shown below each image. Color scale represents range of perfusion values from 0 to 160ml/100g/min. Figure 6C shows the Western analysis for IFNγR and CXCL9 in A498 tumors in representative untreated tumors (un), day 3 of sunitinib (D3), and at the time of resistance (R). Comparisons were performed by Student's T-test.